Polymerase exchange on single DNA molecules reveals processivity clamp control of translesion synthesis

James E. Kath[a], Slobodan Jergic[b], Justin M. H. Heltzel[c,d], Deena T. Jacob[e], Nicholas E. Dixon[b], Mark D. Sutton[c,d], Graham C. Walker[e], and Joseph J. Loparo[a,1]

[a]Department of Biological Chemistry and Molecular Pharmacology, Harvard Medical School, Boston, MA 02115; [b]Centre for Medical and Molecular Bioscience, University of Wollongong, Wollongong, NSW 2522, Australia; [c]Department of Biochemistry and [d]Witebsky Center for Microbial Pathogenesis and Immunology, School of Medicine and Biomedical Sciences, University at Buffalo, State University of New York, Buffalo, NY 14214; and [e]Department of Biology, Massachusetts Institute of Technology, Cambridge, MA 02139

Edited by Richard D. Kolodner, Ludwig Institute for Cancer Research, La Jolla, CA, and approved April 24, 2014 (received for review November 10, 2013)

Translesion synthesis (TLS) by Y-family DNA polymerases alleviates replication stalling at DNA damage. Ring-shaped processivity clamps play a critical but ill-defined role in mediating exchange between Y-family and replicative polymerases during TLS. By reconstituting TLS at the single-molecule level, we show that the *Escherichia coli* β clamp can simultaneously bind the replicative polymerase (Pol) III and the conserved Y-family Pol IV, enabling exchange of the two polymerases and rapid bypass of a Pol IV cognate lesion. Furthermore, we find that a secondary contact between Pol IV and β limits Pol IV synthesis under normal conditions but facilitates Pol III displacement from the primer terminus following Pol IV induction during the SOS DNA damage response. These results support a role for secondary polymerase clamp interactions in regulating exchange and establishing a polymerase hierarchy.

single-molecule techniques | DNA replication | DNA repair | lesion bypass | DinB

Despite the action of several DNA repair pathways, unrepaired damage is encountered by replicative DNA polymerases, which stall at DNA-distorting lesions. Translesion synthesis (TLS), most notably by Y-family polymerases, is one pathway that alleviates such roadblocks. In TLS, a Y-family polymerase switches with a stalled replicative polymerase, synthesizes across from and past the lesion, and then, switches back to allow resumption of normal synthesis (1). The ability of Y-family polymerases to bypass damaged DNA comes at the cost of lower fidelity, requiring careful regulation of polymerase exchange (2).

Processive synthesis by DNA polymerases requires their tethering to the protein-binding cleft of a ring-shaped processivity clamp by a conserved clamp-binding motif (CBM). Canonical clamps, such as the bacterial β and eukaryotic proliferating cell nuclear antigen (PCNA), are multimeric, with a binding cleft on each protomer. Biochemical experiments with bacterial (3, 4) and eukaryotic (5) proteins have suggested that clamps can simultaneously bind multiple DNA polymerases during active DNA synthesis, serving as a molecular toolbelt (6). This multivalency may facilitate rapid polymerase exchange and lesion bypass. However, it remains unclear if and when large multisubunit replicative polymerases can accommodate Y-family polymerases on the clamp. Furthermore, most organisms have multiple Y-family polymerases and many other clamp-binding proteins—at least 10 in *Escherichia coli* (7) and over 50 in humans (8). It is consequently an open question how the correct polymerase is selected at a DNA lesion (1).

To further elucidate the role of processivity clamps in polymerase trafficking, we studied the *E. coli* replicative polymerase, the polymerase (Pol) III heterotrimer αεθ, and the Y-family Pol IV, which individually bind the dimeric β clamp. Pol IV, encoded by the gene *dinB*, is widely conserved across the three domains of life, and it is the homolog of human Pol κ (9). In addition to its function in lesion bypass (10), *E. coli* Pol IV is required for the mechanistically controversial phenomenon of stress-induced mutagenesis (11, 12), which is proposed to occur by its preferential synthesis at double-strand break intermediates (13, 14), and involved in reactive oxygen species-mediated antibiotic lethality by its incorporation of oxidized nucleotides into the genome (15).

Interactions of Pol IV with β and their implications for the toolbelt model have generated widespread interest (4, 16). The structure of the C-terminal little finger domain of Pol IV bound to β revealed that Pol IV can simultaneously interact with the cleft and the rim, a secondary site of β near its dimer interface, which positions the Pol IV catalytic domain well away from the DNA running through the center of the clamp (17). Although this potential inactive binding mode for Pol IV has been interpreted as evidence for the toolbelt model, Pol III was shown to contain a second weak CBM in its ε exonuclease subunit (18) in addition to the CBM in its α catalytic subunit that has a strong affinity for the β clamp. A recent study proposed that Pol III would, therefore, occlude Pol IV from clamp binding during replication, only accommodating simultaneous binding after a lesion-induced stall (19).

Previous efforts to reconstitute this model system for polymerase exchange have involved stalling Pol III on β at a primer terminus by nucleotide omission to synchronize a population of molecules and simulate a lesion-induced block (3, 4). These studies were not able to resolve an exchange back to Pol III after Pol IV synthesis. To bypass these limitations and elucidate the molecular mechanism of exchange between Pol III and Pol IV, we developed a single-molecule assay to observe the whole TLS reaction, quantifying polymerase exchange and bypass at site-specific DNA lesions. Here, we show that Pol III and Pol IV can simultaneously bind β during active synthesis, enabling rapid lesion bypass, and report a previously unidentified inactive

Significance

DNA damage can be a potent block to replication. One pathway to bypass damage is translesion synthesis (TLS) by specialized DNA polymerases. These conserved TLS polymerases have higher error rates than replicative polymerases, requiring careful regulation of polymerase exchange. By reconstituting the full polymerase exchange reaction at the single-molecule level, we show how distinct sets of binding sites on the β processivity clamp regulate exchange between the *Escherichia coli* replicative polymerase (Pol) III and the TLS Pol IV. At low concentrations, Pol IV binds β in an inactive binding mode, promoting rapid bypass of a cognate DNA lesion, whereas at high concentrations (corresponding to SOS damage response levels), association at a low-affinity sites facilitates Pol III displacement.

Author contributions: J.E.K. and J.J.L. designed research; J.E.K. performed research; J.E.K., S.J., J.M.H.H., D.T.J., N.E.D., M.D.S., and G.C.W. contributed new reagents/analytic tools; J.E.K. and J.J.L. analyzed data; and J.E.K., S.J., N.E.D., M.D.S., G.C.W., and J.J.L. wrote the paper.

The authors declare no conflict of interest.

This article is a PNAS Direct Submission.

[1]To whom correspondence should be addressed. E-mail: joseph_loparo@hms.harvard.edu.

This article contains supporting information online at www.pnas.org/lookup/suppl/doi:10.1073/pnas.1321076111/-/DCSupplemental.

binding mode for Pol III. We also observe that, at high concentrations (corresponding to up-regulated levels during the SOS DNA damage response), Pol IV occupies a secondary contact on β, promoting dissociation of Pol III. These results support a model in which secondary contacts between processivity clamps and Y-family polymerases establish a hierarchy for polymerase selection.

Results

Single-Molecule Assay to Measure DNA Polymerase Activity. We used an assay that exploits the differential elasticity of ssDNA and dsDNA to observe primer extension on individual DNA molecules within a microfluidic flow cell (20, 21). Each primed ssDNA substrate, constructed from a 7.2-kb phage M13 genome (Fig. S1*A*), was coupled to a micrometer-scale bead. Laminar flow of buffer through the flow cell exerts a constant force of ~3 pN on the bead and by extension, uniformly throughout the DNA tether. At this low force, ssDNA is entropically coiled, whereas dsDNA is stretched to nearly its crystallographic length (Fig. S1*C*); conversion of ssDNA to dsDNA causes motion of the bead in the direction of buffer flow and can be tracked with high accuracy in space ($\sigma \sim 70$ bp) and time (0.5 s) to determine the amount of DNA synthesized (Fig. 1*A*). DNA synthesis began after the introduction of the components required to reconstitute processive synthesis—polymerase(s), β, the clamp loader complex $\tau_3\delta\delta'\chi\psi$, and nucleotides.

Using this technique, we characterized primer extension by Pol III and Pol IV. Synthesis by either polymerase occurred in discrete steps of processive synthesis interspersed by pauses (Fig. 1*B* and Fig. S1 *E* and *F*). Distributions for the processivity (Fig. 1 *C* and *D*) and rate (Fig. 2*A*) of each synthesis step were generated from a large number of events; the data were in agreement with previous single-molecule experiments for Pol III (22) and bulk data for Pol IV (23). Pauses between synthesis steps were exponentially distributed, consistent with a single rate-limiting step, and we observed that increasing the concentration of Pol III from 5 to 30 nM reduced the pause length (Fig. S2 *A–C*, time constant τ decreases from 19.7 to 12.4 s). Biophysical and structural data suggest that only one Pol III binds the clamp dimer (4, 18, 24, 25), arguing that pauses observed during synthesis result from stochastic dissociation of Pol III from the clamp and the diffusion-limited recruitment of a new polymerase from solution (22).

In contrast, results from structural and biophysical experiments suggest that two Pol IV molecules may simultaneously bind to the dimeric β (4, 17). To test this model, we purified a mutant clamp with a single binding cleft, β^+/β^C (26). Although increasing the concentration of Pol IV from 5 to 30 nM also decreased pauses between Pol IV synthesis steps (Fig. S2 *D–F*, τ decreases from 58.9 to 16.8 s), pausing was not affected by the use of β^+/β^C (Fig. S2*G*). The Pol IV processivity, however, dropped almost in one-half in experiments with β^+/β^C (Fig. S3). Together, these data imply that two Pol IV molecules can occupy β simultaneously but that exchange between the two occurs on a timescale faster than our resolution, increasing the apparent processivity. Similar to Pol III, the concentration-dependent pauses observed result from recruitment of a Pol IV molecule to the clamp from solution.

Observation of Pol III–Pol IV Exchange and Lesion Bypass. The dramatically different rates of the two polymerases (Fig. 2*A*) enable assignment of synthesis events to either Pol III or Pol IV. We, therefore, performed primer extension with a mixture of Pol III (5 nM) and Pol IV (30 nM). This ratio was chosen to approximate that found in cells during exponential growth (2), with concentrations reduced (from about 20 nM for Pol III and 300 nM for Pol IV) so that distinct synthesis events could be resolved. If the fraction of active protein differs for each one, then the molar ratio of active polymerases will be shifted by a constant factor. Under these conditions, Pol III performed 78% of DNA synthesis (Fig. S4), likely because of stronger interactions with β (2); however, one or more Pol IV events were also observed in 75% of trajectories (Fig. 2*B*), exchanging with Pol III.

To observe polymerase exchange in the physiological context of a DNA lesion, we adapted a protocol (27) to generate single-stranded M13 substrates with a site-specific N^2-furfuryl-dG adduct: a cognate lesion for Pol IV (Fig. S1*B*). N^2-furfuryl-dG is a minor groove lesion that is efficiently and accurately bypassed by Pol IV and an analog of the primary adduct formed by the antibiotic nitrofurazone, an agent to which Pol IV KO strains are significantly sensitive (10).

Although the lesion strongly blocked Pol III in ensemble synthesis in the absence of the clamp (Fig. S5*A*), we found that it blocked only 65% of trajectories in single-molecule experiments (Fig. 3*A* and Fig. S5*B*). Previous studies have shown that Pol III lesion bypass efficiency is strongly promoted by β (28) and increased dNTP levels, which bias polymerase over exonuclease activity (29); we, indeed, observed that higher dNTP levels increased bypass (Fig. S5*B*). The addition of both polymerases to the primer extension reaction alleviated the block at the N^2-furfuryl-dG position (Fig. 3*A*) and revealed polymerase exchange at the lesion site and bypass by Pol IV (Fig. 3*B*).

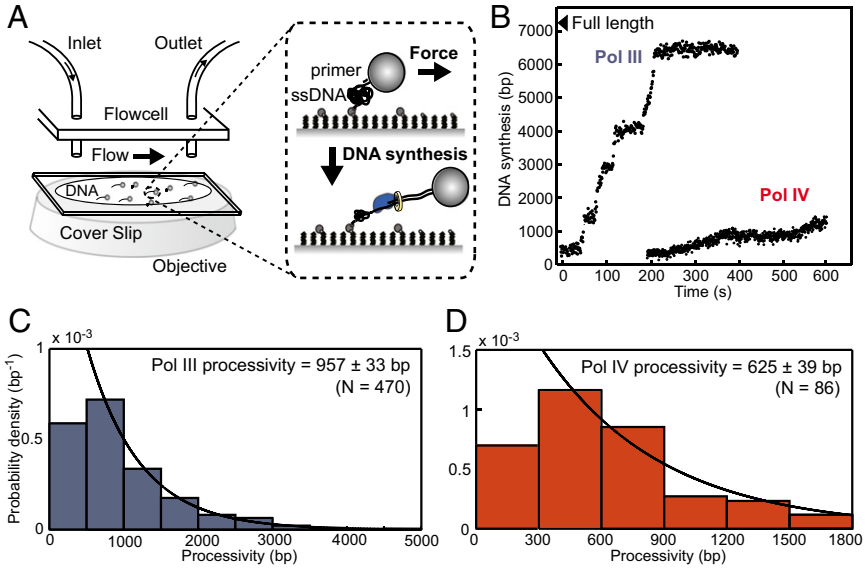

Fig. 1. A single-molecule primer extension assay. (*A*) Under an applied force of ~3 pN, ssDNA is entropically collapsed, whereas dsDNA is extended to nearly its crystallographic length. Primer extension results in motion of tethered beads in the direction of flow. (*B*) Representative trajectories of synthesis by Pol III and Pol IV on individual DNA molecules (Fig. S1 *E* and *F*). (*C* and *D*) Processivity distributions for (*C*) Pol III (5 nM) and (*D*) Pol IV (30 nM); values represent means ± SEMs.

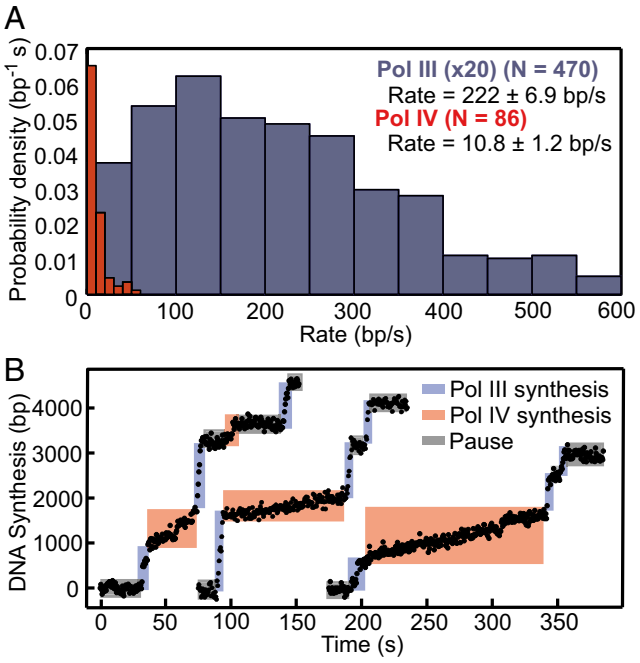

Fig. 2. Observing exchange between Pol III and Pol IV. (*A*) Rate distributions for Pol III (blue) and Pol IV (red); values represent means ± SEMs. Probability densities for Pol III are multiplied by 20 to facilitate comparison. (*B*) Sample trajectories of rapid exchange between Pol III and Pol IV.

Kinetics of Polymerase Exchange Support the Toolbelt Model. The observation of exchange from Pol III to Pol IV and back is uniquely accessible in our single-molecule reconstitution and permits us to investigate the role of β in polymerase trafficking. In the toolbelt model, polymerase exchange is only limited by the timescale of conformational changes of Pol III and Pol IV simultaneously bound to β. In an alternative model, in which steric effects prevent concurrent binding, exchange requires dissociation of the first polymerase followed by recruitment of the second from solution, which would be sensitive to protein dilution. Quantifying exchange by measuring the time between the termination of synthesis by one polymerase and the subsequent initiation of synthesis by the other allows us to distinguish between these two models.

The time for exchange from Pol III to Pol IV on undamaged DNA (Fig. 4*C*) was more rapid than the diffusion-limited recruitment time of Pol IV from solution (Fig. 4*A* and Fig. S2) seen in exponential fits and a statistical comparison of the two datasets ($P < 10^{-5}$) (*SI Experimental Procedures*). Furthermore, reducing the concentration of Pol IV in exchange experiments from 30 to 15 nM did not affect the timescale of exchange (Fig. S6), whereas the same dilution increased pause times in experiments with Pol IV alone (Fig. 4*A* and Fig. S2*E*). These data argue that exchange during active synthesis occurs between two polymerases bound to the clamp. Our observation of β-mediated exchange implies that the second Pol III CBM in the ε subunit does not exclude Pol IV from binding the clamp in the absence of a lesion-induced stall in contrast to a previous suggestion (19); rather, Pol IV can compete with ε for a cleft, allowing Pol IV to bind β while Pol III is synthesizing DNA.

Importantly, we observed that exchange back to Pol III after Pol IV synthesis was also more rapid than the recruitment time of Pol III from solution (Fig. 4 *B* and *D*) ($P < 10^{-9}$). Furthermore, exchange from Pol IV to Pol III in the presence of the single-cleft β^{+}/β^{C} (Fig. S7*A*, $\tau = 27.3$ s) was slower than in experiments with the WT clamp ($P < 10^{-3}$), closely matching the recruitment time of Pol III from solution [not significant (NS) vs. Fig. 4*B*]. These data show that Pol III can bind the opposing cleft of β in an inactive conformation while Pol IV is carrying out synthesis and that eliminating the second cleft abolishes rapid exchange. The fact that the Pol IV processivity preceding exchange to Pol III matches that of Pol IV on β^{+}/β^{C} (Figs. S3*B* and S7*B*) shows that a single Pol IV is bound to β in the presence of Pol III and strongly implies that Pol III does not displace Pol IV during the exchange back but takes over after Pol IV stochastically releases DNA.

To test if polymerase exchange can occur in the physiological context of Pol III encountering a DNA lesion, we collected data for exchange from Pol III to Pol IV within the experimental resolution (±200 bp) of the N^2-furfuryl-dG position (Fig. 3*B*). These exchange times (Fig. 4*E*) matched the times for exchange on undamaged DNA (*NS* vs. Fig. 4*C*) and were more rapid than recruitment of Pol IV from solution ($P < 0.01$ vs. Fig. 4*A*), indicating that Pol IV was bound to β when Pol III encountered the lesion. The switch back to Pol III after the lesion (Fig. 4*F*) was intermediate between rapid β-mediated exchange and recruitment from solution, suggesting a mixture of these two types of exchange.

Binding of Pol IV at a Secondary Site on β Reduces the Pol III Processivity. Our results support a model in which Pol IV, at a ratio to Pol III consistent with normal growth, can bind β in an inactive conformation, thereby promoting rapid bypass of DNA lesions encountered during synthesis. During the SOS DNA damage response, however, the cellular concentration of Pol IV increases roughly 10-fold, whereas Pol III levels remain constant (2). To test if an increased ratio of Pol IV to Pol III alters polymerase exchange, we performed primer extension experiments with 5 nM Pol III and 300 nM Pol IV. At these

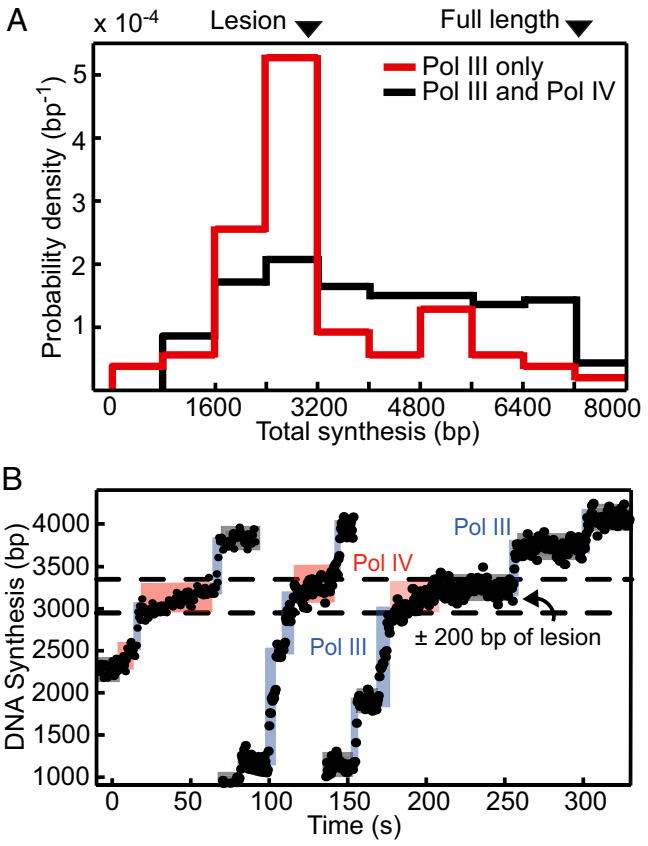

Fig. 3. A single-molecule reconstitution of polymerase exchange and bypass at a DNA lesion. (*A*) An N^2-furfuryl-dG lesion at ~3,150 bp blocks processive synthesis by Pol III (5 nM; $n = 69$) but is bypassed when Pol IV (30 nM) is added ($n = 175$). (*B*) Rapid exchange from Pol III to Pol IV and back is observed at the lesion site.

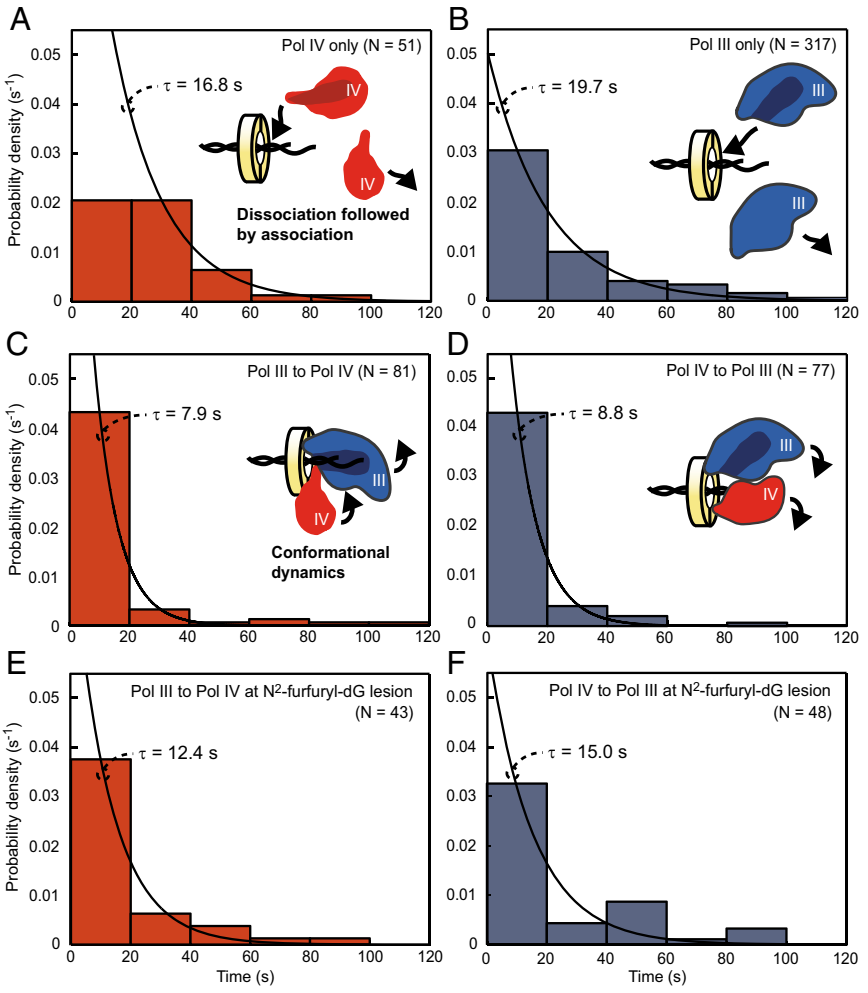

Fig. 4. β acts as a molecular toolbelt for Pol III and Pol IV to promote lesion bypass. Each distribution is fit to an exponential with associated time constant τ. Pauses represent association of a new polymerase from solution in experiments with (*A*) Pol IV (30 nM) or (*B*) Pol III alone (5 nM). (*C*) Exchange from Pol III (5 nM) to Pol IV (30 nM; $P < 10^{-5}$ vs. *A*) and (*D*) back to Pol III ($P < 10^{-9}$ vs. *B*) is rapid because of simultaneous binding of both polymerases to the clamp. (*E*) Exchange to Pol IV at the N^2-furfuryl-dG site is also rapid ($P < 0.01$ vs. *A* and *NS* vs. *C*), indicating that lesion bypass is β-mediated. (*F*) Exchange back to Pol III is intermediate between *B* ($P = 0.04$) and *D* ($P = 0.02$), suggesting that both types of exchange occur. *SI Experimental Procedures* has additional analysis.

concentrations, Pol IV outcompeted Pol III, performing 78% of DNA synthesis (Fig. S4). Although the average processivity of Pol III synthesis preceding exchange was only modestly affected by Pol IV under normal conditions, possibly because of disruption of the binding of the ε subunit of Pol III to β (Fig. S8*A*), under SOS-like conditions, it dropped almost by half (Fig. 5*A*) ($P < 10^{-5}$), reflecting a decrease of the lifetime of Pol III on the clamp (Fig. S8*B*). This reduction in processivity was dose-dependent with the Pol IV concentration and β-mediated; Pol IV^C, a mutant that lacks its CBM, did not reduce the Pol III processivity (Fig. 5*A*).

To further define which interactions with β mediate this activity, we tested the effects of mutant clamps under SOS-like conditions; β^R, a clamp mutant that weakens the secondary Pol IV–β-interaction at the rim site (4), did not affect the synthesis of Pol III alone but partially restored the Pol III processivity at a high Pol IV concentration (Fig. 5*B*) ($P < 0.01$). Although the processivity of Pol III was reduced slightly with the single-cleft β^+/β^C, consistent with the model that the ε subunit stabilizes it on the clamp (18, 19), a high concentration of Pol IV with β^+/β^C reduced the Pol III processivity equivalently to the WT clamp condition (Fig. 5*B*), further supporting a role for the noncleft rim contact in Pol III displacement.

Discussion

By visualizing the TLS reaction in its entirety at the single-molecule level, our data provide a comprehensive view of how Pol IV access to the replication fork is regulated through interactions with β (Fig. 6). Pol IV, at relatively low concentrations during normal growth, is able to associate with the rim site and compete with the weakly bound ε subunit of Pol III for its cleft (Fig. 4). By occupying the rim and cleft sites of β in an inactive mode during normal growth conditions, Pol IV is available for rapid exchange and translesion synthesis when Pol III stalls on encountering a lesion, which was proposed in the toolbelt model (6).

We have also shown that a previously unidentified inactive binding mode for Pol III allows it to remain bound to the cleft of one protomer of β until the switch back (Fig. 4 and Fig. S7*A*), the other half of the polymerase exchange reaction that has been difficult to resolve by bulk biochemical studies (3, 4). The Pol IV processivity preceding a switch back to Pol III is not reduced from that of Pol IV alone (Fig. S7*B*), suggesting that Pol III does not actively displace Pol IV during translesion synthesis but relies on the lower processivity of Pol IV to minimize the mutagenic load.

At higher concentrations of Pol IV (corresponding to the SOS damage response), we observed a decrease in the Pol III processivity (Fig. 5*A*). We propose that this decrease is caused by an increased occupancy of Pol IV at the low-affinity rim sites of β (Fig. 6). Adjacent to the Pol III α subunit, Pol IV would be positioned to dynamically replace the strongly bound CBM of α during a transient release from the cleft, which can be seen in a molecular model of both polymerases bound to β (Fig. S9). This role for the rim contact is consistent with biochemical results that β^+/β^C can support polymerase exchange to Pol IV when Pol III is stalled by nucleotide omission (4). Without the critical α–β contact after cleft capture by Pol IV, Pol III would dissociate from the primer terminus, allowing Pol IV to take its place. Unless the displaced Pol III could bind an adjacent

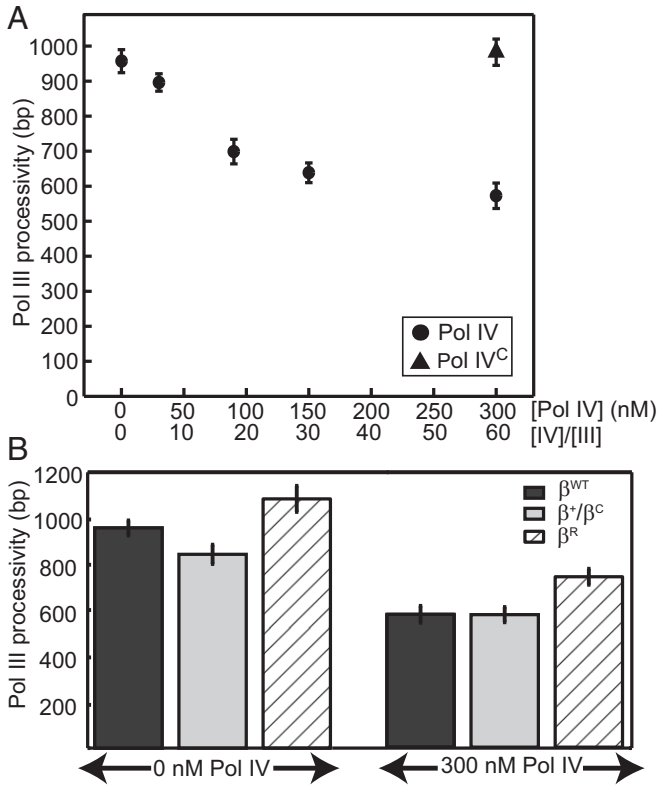

Fig. 5. Binding of Pol IV at a secondary site on β reduces the Pol III processivity. (*A*) The Pol III processivity decreases with increasing concentrations of Pol IV (●) but is unaffected by Pol IV^C, a mutant lacking its CBM (▲). (*B*) Reduction in the Pol III processivity with β^{WT} (black bars) also occurs with the single-cleft mutant clamp β^+/β^C (gray bars; *NS*) but is partially alleviated by β^R, a clamp with a weakened Pol IV-interacting rim interface (cross-hatched bars; $P < 0.01$). *N* ranges from 71 to 470 for *A* and *B*, respectively. Values represent means ± SEMs.

unoccupied protomer or is stabilized by additional interactions, it would likely dissociate from the clamp entirely.

The requirement of the Pol IV CBM indicates that binding at rim sites is not sufficient for a reduction of the Pol III lifetime on DNA and that Pol IV must also compete for the cleft bound by α. Shared contacts, such as a single cleft of β during competition between Pol III and Pol IV bound at additional sites on β, have been proposed to be important in facilitating dissociation and subunit exchange in multiprotein complexes upon transient contact release (30). This phenomenon has also been observed in the dynamic processivity of phage T4 and T7 replication, where additional polymerases are able to associate with moving replisomes and undergo exchange on a timescale faster than that of stochastic dissociation of the synthesizing polymerase (31–33), and the facilitated dissociation of the *E. coli* DNA-binding protein Fis by nucleoid proteins (34). Secondary contacts, such as the rim site for Pol IV shown here, play an important role in orienting proteins to exploit transient changes in occupancy of these shared sites, resulting in binding partner exchange.

During coordinated leading and lagging strand replication, a displaced Pol III may remain associated with the replisome through additional contacts with the clamp loader complex. These contacts, however, do not seem to prevent Pol IV from accessing β; previous biochemical experiments with a fully reconstituted replisome have shown that Pol IV can replace Pol III (35). Furthermore, overexpression of Pol IV beyond SOS levels in cells has been shown to arrest replication and induce toxicity because of unregulated access of Pol IV to the replication fork (15, 35, 36). Removing the CBM residues alleviates Pol IV toxicity, whereas mutating the rim-contacting residues partially alleviates it (16). These data are explained by our model: contacts with the rim site and subsequently, the cleft provide a molecular path for Pol IV to displace Pol III from the primer terminus after SOS induction.

A putative interaction with the rim site could also position the other *E. coli* Y-family polymerase, Pol V, on the clamp when it is expressed later in the SOS damage response (37). This binding activity would create a hierarchy for access to the primer terminus, a view of the toolbelt model in which clamp–polymerase interactions do more than merely increase the local polymerase concentration at the DNA template. During normal growth conditions, Pol III, which is preferentially loaded to the primer terminus (38), performs the majority of DNA synthesis. Pol IV is able to simultaneously bind β in an inactive mode, although it is currently unclear how other β-interacting proteins would influence its occupancy in vivo. After SOS induction, the rim site positions Pol IV to preferentially bind a cleft of β when it becomes available. Such a competitive advantage would ensure timely access of Y-family polymerases to the primer template and is likely to be important with several proteins competing for an open cleft.

Noncleft contacts may play a similar role in regulating access to the DNA template in other domains of life. PCNA plays a key role in coordinating the handoff of DNA intermediates between a polymerase, flap endonuclease, and ligase during both Okazaki fragment maturation and long-patch base excision repair in eukaryotes (39). Structural studies have revealed that Flap endonuclease-1, Polymerase β, and Ligase I bind overlapping but distinct regions of DNA intermediates, which may facilitate displacement during handoff (40). In the archaeon *Sulfolobus solfataricus*, the three enzymes each bind distinct monomers of the heterotrimeric PCNA during Okazaki fragment maturation (41). However suggestive, it remains unknown if the homotrimeric eukaryotic PCNA can simultaneously bind any combination of these three proteins.

Eukaryotic TLS is regulated, in part, by ubiquitination of PCNA; all four human Y-family polymerases have ubiquitin-binding domains (1). Structural data of monoubiquitinated PCNA and its conformations support the model that the secondary ubiquitin site allows the TLS polymerase Pol η to bind an occupied clamp and position it to compete for the cleft on transient dissociation of the replicative polymerase (42, 43). In contrast to bacteria, where the occupancy of the rim site is controlled by polymerase concentration, analogous sites in eukaryotes are introduced by posttranslational modification. We anticipate that the single-molecule approaches described here will serve as powerful tools to elucidate the role of these interactions in translesion synthesis.

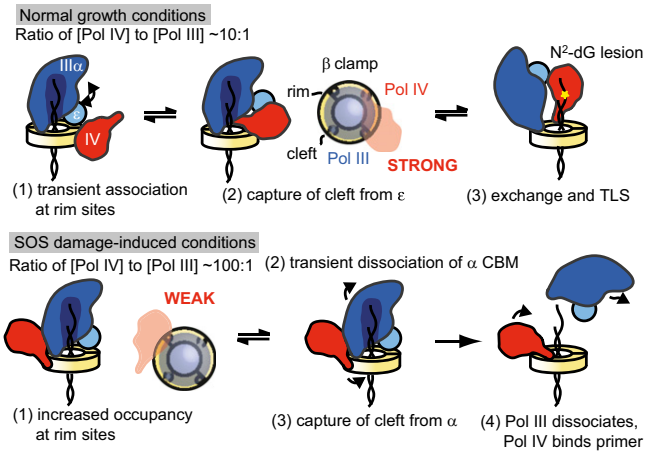

Fig. 6. A model for how the Pol IV occupancy at rim sites and competition with Pol III subunits dictate polymerase exchange at different Pol IV concentrations. The small θ subunit of Pol III, which binds ε, is not represented for clarity.

Experimental Procedures

Proteins and Buffers. Pol III core ($\alpha\varepsilon\theta$), Pol IV, β (WT and mutants), and other *E. coli* replisome components were expressed and purified as described in *SI Experimental Procedures*. Experiments were performed in replication buffer [50 mM Hepes-KOH, pH 7.9, 12 mM $Mg(OAc)_2$, 80 mM KCl, 0.1 mg mL^{-1} BSA] with 5 mM DTT, 1 mM ATP, 760 μM dNTPs, 15 nM $\tau_3\delta\delta'\chi\psi$, 30 nM clamp ($\beta$, β^R, or β^+/β^C as dimers), and the indicated concentrations of Pol III and/or Pol IV; 60 μM dNTPs were used for single-molecule lesion bypass experiments. Single-stranded DNA-binding (SSB) protein was excluded from primer extension experiments, because SSB protein extends ssDNA at low force, reducing the contrast with dsDNA that is used to observe replication (44).

ssDNA Constructs. DNA constructs were generated from circular M13 ssDNA with either M13mp18 ssDNA (New England Biolabs) or purified M13mp7(L2) containing a site-specific N^2-furfuryl-dG lesion and constructed using a previously described protocol (27). M13mp7(L2) phage stock was a gift from John Essigmann (Massachusetts Institute of Technology, Cambridge, MA). Additional details on substrate construction and a list of oligonucleotides used (Table S1) can be found in *SI Experimental Procedures*.

Single-Molecule Experiments. Single-molecule primer extension experiments were performed in custom microfluidic flow cells constructed with functionalized glass coverslips as described previously (45). Statistical comparisons were made between full datasets with the two-tailed Wilcoxon rank sum test using the Matlab function ranksum. A significance level of $P = 0.05$ was used. Additional details on the experimental approach and data analysis are described in *SI Experimental Procedures*.

ACKNOWLEDGMENTS. We thank Jamie Foti for providing purified Pol IV, Deyu Li for assistance with purifying the N^2-furfuryl-dG oligonucleotide, and Johannes Walter and Seungwoo Chang for helpful discussions and critical reading of the manuscript. This work was funded by National Institutes of Health Grants T32 GM008313 (to J.E.K.), R01 GM066094 (to M.D.S.), R01 CA021615 (to G.C.W.), and P30ES002019 (to G.C.W.); a National Science Foundation Graduate Research Fellowship (to J.E.K.); the Smith Family Award in Biomedical Excellence (to J.J.L.); the Stuart Trust Fellows Award (to J.J.L.); and Australian Research Council Grant DP0877658, including an Australian Professorial Fellowship (to N.E.D.). G.C.W. is an American Cancer Society Professor.

1. Sale JE, Lehmann AR, Woodgate R (2012) Y-family DNA polymerases and their role in tolerance of cellular DNA damage. *Nat Rev Mol Cell Biol* 13(3):141–152.
2. Sutton MD (2010) Coordinating DNA polymerase traffic during high and low fidelity synthesis. *Biochim Biophys Acta* 1804(5):1167–1179.
3. Indiani C, McInerney P, Georgescu R, Goodman MF, O'Donnell M (2005) A sliding-clamp toolbelt binds high- and low-fidelity DNA polymerases simultaneously. *Mol Cell* 19(6):805–815.
4. Heltzel JM, Maul RW, Scouten Ponticelli SK, Sutton MD (2009) A model for DNA polymerase switching involving a single cleft and the rim of the sliding clamp. *Proc Natl Acad Sci USA* 106(31):12664–12669.
5. Zhuang Z, et al. (2008) Regulation of polymerase exchange between Pol eta and Pol delta by monoubiquitination of PCNA and the movement of DNA polymerase holoenzyme. *Proc Natl Acad Sci USA* 105(14):5361–5366.
6. Pagès V, Fuchs RP (2002) How DNA lesions are turned into mutations within cells? *Oncogene* 21(58):8957–8966.
7. Wijffels G, et al. (2004) Inhibition of protein interactions with the β_2 sliding clamp of *Escherichia coli* DNA polymerase III by peptides from β_2-binding proteins. *Biochemistry* 43(19):5661–5671.
8. Moldovan GL, Pfander B, Jentsch S (2007) PCNA, the maestro of the replication fork. *Cell* 129(4):665–679.
9. Ohmori H, et al. (2001) The Y-family of DNA polymerases. *Mol Cell* 8(1):7–8.
10. Jarosz DF, Godoy VG, Delaney JC, Essigmann JM, Walker GC (2006) A single amino acid governs enhanced activity of DinB DNA polymerases on damaged templates. *Nature* 439(7073):225–228.
11. McKenzie GJ, Lee PL, Lombardo MJ, Hastings PJ, Rosenberg SM (2001) SOS mutator DNA polymerase IV functions in adaptive mutation and not adaptive amplification. *Mol Cell* 7(3):571–579.
12. Slechta ES, et al. (2003) Adaptive mutation: General mutagenesis is not a programmed response to stress but results from rare coamplification of *dinB* with *lac*. *Proc Natl Acad Sci USA* 100(22):12847–12852.
13. Ponder RG, Fonville NC, Rosenberg SM (2005) A switch from high-fidelity to error-prone DNA double-strand break repair underlies stress-induced mutation. *Mol Cell* 19(6):791–804.
14. Pomerantz RT, Kurth I, Goodman MF, O'Donnell ME (2013) Preferential D-loop extension by a translesion DNA polymerase underlies error-prone recombination. *Nat Struct Mol Biol* 20(6):748–755.
15. Foti JJ, Devadoss B, Winkler JA, Collins JJ, Walker GC (2012) Oxidation of the guanine nucleotide pool underlies cell death by bactericidal antibiotics. *Science* 336(6079):315–319.
16. Wagner J, Etienne H, Fuchs RP, Cordonnier A, Burnouf D (2009) Distinct β-clamp interactions govern the activities of the Y family PolIV DNA polymerase. *Mol Microbiol* 74(5):1143–1151.
17. Bunting KA, Roe SM, Pearl LH (2003) Structural basis for recruitment of translesion DNA polymerase Pol IV/DinB to the β-clamp. *EMBO J* 22(21):5883–5892.
18. Jergic S, et al. (2013) A direct proofreader-clamp interaction stabilizes the Pol III replicase in the polymerization mode. *EMBO J* 32(9):1322–1333.
19. Toste Rêgo A, Holding AN, Kent H, Lamers MH (2013) Architecture of the Pol III-clamp-exonuclease complex reveals key roles of the exonuclease subunit in processive DNA synthesis and repair. *EMBO J* 32(9):1334–1343.
20. Wuite GJ, Smith SB, Young M, Keller D, Bustamante C (2000) Single-molecule studies of the effect of template tension on T7 DNA polymerase activity. *Nature* 404(6773):103–106.
21. Maier B, Bensimon D, Croquette V (2000) Replication by a single DNA polymerase of a stretched single-stranded DNA. *Proc Natl Acad Sci USA* 97(22):12002–12007.
22. Tanner NA, et al. (2008) Single-molecule studies of fork dynamics in *Escherichia coli* DNA replication. *Nat Struct Mol Biol* 15(2):170–176.
23. Wagner J, Fujii S, Gruz P, Nohmi T, Fuchs RP (2000) The β clamp targets DNA polymerase IV to DNA and strongly increases its processivity. *EMBO Rep* 1(6):484–488.
24. Lamers MH, Georgescu RE, Lee S-G, O'Donnell M, Kuriyan J (2006) Crystal structure of the catalytic α subunit of *E. coli* replicative DNA polymerase III. *Cell* 126(5):881–892.
25. Ozawa K, et al. (2013) Proofreading exonuclease on a tether: The complex between the E. coli DNA polymerase III subunits α, epsilon, θ and β reveals a highly flexible arrangement of the proofreading domain. *Nucleic Acids Res* 41(10):5354–5367.
26. Scouten Ponticelli SK, Duzen JM, Sutton MD (2009) Contributions of the individual hydrophobic clefts of the *Escherichia coli* β sliding clamp to clamp loading, DNA replication and clamp recycling. *Nucleic Acids Res* 37(9):2796–2809.
27. Delaney JC, Essigmann JM (2006) Assays for determining lesion bypass efficiency and mutagenicity of site-specific DNA lesions *in vivo*. *Methods Enzymol* 408:1–15.
28. Tomer G, Reuven NB, Livneh Z (1998) The β subunit sliding DNA clamp is responsible for unassisted mutagenic translesion replication by DNA polymerase III holoenzyme. *Proc Natl Acad Sci USA* 95(24):14106–14111.
29. Gon S, Napolitano R, Rocha W, Coulon S, Fuchs RP (2011) Increase in dNTP pool size during the DNA damage response plays a key role in spontaneous and induced-mutagenesis in *Escherichia coli*. *Proc Natl Acad Sci USA* 108(48):19311–19316.
30. Ha T (2013) Single-molecule approaches embrace molecular cohorts. *Cell* 154(4):723–726.
31. Yang J, Zhuang Z, Roccasecca RM, Trakselis MA, Benkovic SJ (2004) The dynamic processivity of the T4 DNA polymerase during replication. *Proc Natl Acad Sci USA* 101(22):8289–8294.
32. Hamdan SM, et al. (2007) Dynamic DNA helicase-DNA polymerase interactions assure processive replication fork movement. *Mol Cell* 27(4):539–549.
33. Loparo JJ, Kulczyk AW, Richardson CC, van Oijen AM (2011) Simultaneous single-molecule measurements of phage T7 replisome composition and function reveal the mechanism of polymerase exchange. *Proc Natl Acad Sci USA* 108(9):3584–3589.
34. Graham JS, Johnson RC, Marko JF (2011) Concentration-dependent exchange accelerates turnover of proteins bound to double-stranded DNA. *Nucleic Acids Res* 39(6):2249–2259.
35. Indiani C, Langston LD, Yurieva O, Goodman MF, O'Donnell M (2009) Translesion DNA polymerases remodel the replisome and alter the speed of the replicative helicase. *Proc Natl Acad Sci USA* 106(15):6031–6038.
36. Uchida K, et al. (2008) Overproduction of Escherichia coli DNA polymerase DinB (Pol IV) inhibits replication fork progression and is lethal. *Mol Microbiol* 70(3):608–622.
37. Beuning PJ, Sawicka D, Barsky D, Walker GC (2006) Two processivity clamp interactions differentially alter the dual activities of UmuC. *Mol Microbiol* 59(2):460–474.
38. Downey CD, McHenry CS (2010) Chaperoning of a replicative polymerase onto a newly assembled DNA-bound sliding clamp by the clamp loader. *Mol Cell* 37(4):481–491.
39. Chapados BR, et al. (2004) Structural basis for FEN-1 substrate specificity and PCNA-mediated activation in DNA replication and repair. *Cell* 116(1):39–50.
40. Tsutakawa SE, et al. (2011) Human flap endonuclease structures, DNA double-base flipping, and a unified understanding of the FEN1 superfamily. *Cell* 145(2):198–211.
41. Beattie TR, Bell SD (2012) Coordination of multiple enzyme activities by a single PCNA in archaeal Okazaki fragment maturation. *EMBO J* 31(6):1556–1567.
42. Freudenthal BD, Gakhar L, Ramaswamy S, Washington MT (2010) Structure of monoubiquitinated PCNA and implications for translesion synthesis and DNA polymerase exchange. *Nat Struct Mol Biol* 17(4):479–484.
43. Tsutakawa SE, et al. (2011) Solution X-ray scattering combined with computational modeling reveals multiple conformations of covalently bound ubiquitin on PCNA. *Proc Natl Acad Sci USA* 108(43):17672–17677.
44. Fu H, Le S, Chen H, Muniyappa K, Yan J (2013) Force and ATP hydrolysis dependent regulation of RecA nucleoprotein filament by single-stranded DNA binding protein. *Nucleic Acids Res* 41(2):924–932.
45. Tanner NA, van Oijen AM (2010) Visualizing DNA replication at the single-molecule level. *Methods Enzymol* 475:259–278.

Supporting Information

Kath et al. 10.1073/pnas.1321076111

SI Experimental Procedures

Proteins and Buffers. *Escherichia coli* proteins were purified from overproducing strains as previously described and untagged unless otherwise noted: polymerase (Pol) IV (1) and Pol IV^{C} (ΔC5) (2); the Pol III holoenzyme subunits α, δ, and δ′ (3); ε and θ (4); the WT clamp β (5), N-terminally his$_6$- and heart muscle kinase-tagged β^{R} (E93K-L98K), and β^{+}/β^{C}, a stable dimer formed from N-terminally Myc-tagged β and his$_6$- and heart muscle kinase-tagged β(ΔC5) (6); and τ and refolded ψ within the χψ-complex (7). The Pol III αεθ core and clamp loader assembly with the stoichiometry $\tau_3\delta\delta'\chi\psi$ were each reconstituted and purified following reported protocols (7).

The quality of purified protein was determined by comparing the activities of multiple preparations. A fraction of inactive or misfolded polymerases, inevitable in purification, would either fail to bind the clamp and not be observed in synthesis or bind and result in termination events or extended pauses. Because our conclusions depend on the reduction of pause times because of polymerase exchange, they are unlikely to be affected by inactive protein. If the fractions of active protein in the Pol III and Pol IV preparations used differed, the molar ratio of active Pol IV to active Pol III would differ from the ratio determined by protein concentration (Fig. 5) by a constant factor throughout this work and similarly not affect our conclusions.

Synthesis of an N^2-furfuryl-dG–Containing Oligonucleotide. The 20-mer oligonucleotide containing the N^2-furfuryl-dG lesion was constructed as previously described (8). A 20-mer oligonucleotide containing a fluoro substituent at the N^2 position of guanine (**X**) was purchased from Chemgenes: 5′-CTA CCT **X**TG GAC GGC TGC GA-3′. A fraction of the product was found to contain a hydroxyl group in place of the fluorine, the result of NaOH treatment to separate the oligonucleotide from the resin during manufacture. The fluorine was displaced with a fufuryl group by treating the oligonucleotide with fufurylamine, leaving the contaminating N^2-hydroxyl-dG unaffected. Fufurylamine treatment was followed by HPLC and MALDI-TOF MS as described (8) to remove the hydroxyl-containing oligonucleotide to obtain a pure 20-mer with the N^2-fufuryl-dG lesion.

M13 ssDNA with a Site-Specific DNA Lesion. ssDNA with a site-specific DNA lesion was constructed using M13mp7(L2), a mutant phage that contains an EcoRI site within a stable hairpin in its genome (Fig. S1*B*). Phage stock was a gift from John Essigmann (Massachusetts Institute of Technology, Cambridge, MA). A protocol to purify phage genomes and ligate a lesion-containing oligonucleotide at the digested EcoRI site (9) was adapted for this study with the following modifications. After PEG precipitation, the isolated phage pellet was extracted two or three times with 25:24:1 phenol:chloroform:isoamyl alcohol and one time with pure chloroform. DNA in the final aqueous layer was ethanol-precipitated and redissolved in 10 mM Tris (pH 8.5) buffer to ∼2 μg μL^{-1}; 100 μg M13mp7(L2) DNA was linearized in a 100-μL digestion reaction with 40 U EcoRI-HF (New England Biolabs) and 1× Buffer 4 at 23 °C for 8 h and purified with sequential phenol:chloroform:isoamyl alcohol and chloroform extractions and an ethanol precipitation. Then, it was dissolved in 100 μL Tris buffer. Purification of linear ssDNA prevented degradation in later steps.

Thirty picomoles 5′-phosphorylated oligonucleotide insert 5′-CTA CCT **X**TG GAC GGC TGC GA-3′ (**X** = N^2-furfuryl-dG or the dG control) was ligated at 16 °C overnight into 20 pmol purified linear ssDNA using annealed scaffold oligonucleotides 5′-AAA ACG ACG GCC AGT GAA TTT CGC AGC CGT CC-3′ and 5′-GGT AGA CTG AAT CAT GGT CAT AGC-3′ (25 pmol each) and 800 U T4 DNA ligase (New England Biolabs) in a 60-μL reaction. To remove the scaffold oligonucleotides, unligated linear M13 DNA, and excess insert, the mixture was subsequently treated at 37 °C for 4 h with 18 U T4 DNA polymerase and 80 U exonuclease I (New England Biolabs). The DNA was finally purified by sequential phenol:chloroform:isoamyl alcohol and chloroform extractions, ethanol-precipitated, and dissolved in 50 μL 10 mM Tris buffer to obtain the lesion-containing (or control) phage ssDNA.

The progress of DNA construction was monitored by taking samples at each step and separating them on a 0.8% Tris-acetate-EDTA agarose gel stained with ethidium bromide (Fig. S5*C*). As a control to guarantee that EcoRI completely linearized the hairpin-containing M13mp7(L2) ssDNA, which if uncut, could contaminate lesion-containing DNA, a mock ligation reaction was performed with digested ssDNA and scaffolds but without the insert. The mock reaction was then treated with T4 DNA polymerase and Exo I, which together degrade linear but not circular ssDNA. Degradation was nearly complete, showing efficient digestion of the hairpin (Fig. S5*C*).

Single-Molecule DNA Substrates. Linear end-labeled single-molecule DNA substrates were constructed using circular 7.2-kb M13 phage genomes (Fig. S1*A*). Experiments on undamaged DNA used substrates generated from M13mp18 ssDNA (New England Biolabs). Sixteen microliters this DNA (250 ng μL^{-1}) was annealed in 20 μL with 1 μM oligonucleotide mp18-SalI (Table S1) by heating to 65 °C for 10 min and slowly cooling to room temperature. Ten microliters annealed DNA was linearized at the dsDNA region with 10 U SalI (New England Biolabs) and 1× Buffer 3 in 50 μL at 37 °C for 1 h. Forty microliters restriction digest reaction was mixed to a final volume of 55 μL with 30 nM end-labeled oligonucleotides M13-5′-biotin and phosphorylated M13-3′-dig and 30 nM scaffolding oligonucleotides mp18-scaffold-1 and mp18-scaffold-2 (Table S1). The scaffolds were annealed to the linearized phage DNA and the end-labeled oligonucleotides by heating to 65 °C for 20 min and cooling to room temperature, also inactivating SalI; scaffold-mediated ligation was subsequently performed overnight at 16 °C with 400 U DNA ligase (New England Biolabs). The reaction was stopped by heat-inactivating ligase at 65 °C for 10 min and adding EDTA (20 mM final) to the cooled mixture. The stock solution (final substrate concentration ∼ 5 nM) was stored at 4 °C.

Single-molecule DNA substrates containing a site-specific lesion (Fig. S1*B*) were prepared similarly from lesion-containing M13mp7(L2) DNA (see above). ssDNA containing the N^2-furfuryl-dG lesion or the control dG was annealed with mp7L2-AlwNI (Table S1) and digested with 20 U AlwNI (New England Biolabs) in 1× Buffer 4 at 37 °C for 1 h. Linearized DNA was ligated to M13-5′-biotin and phosphorylated M13-3′-dig using the scaffolding oligonucleotides mp7L2-scaffold-1 and mp7L2-scaffold-2 (Table S1).

The annealed oligonucleotide mp18-scaffold-1 (for the undamaged substrate) or mp7L2-scaffold-1 (for the lesion-containing substrate) near the 3′ terminus of the linear M13 template served as the primer for DNA synthesis. For the lesion-containing substrate, the primer terminus is situated ∼3,150 nt from the N^2-furfuryl-dG site.

Single-Molecule Flow Stretching Experiments. Single-molecule experiments were performed at 23 °C using custom microfluidic

flow cells with glass coverslips as described previously (10). In summary, primed end-labeled M13 bacteriophage ssDNA was attached to the glass surface of the flow cell by a biotin-streptavidin linkage on one end and a micrometer-scale bead (tosyl-activated, 2.8-μm diameter; Dynal) by a digoxigenin–antidigoxigenin interaction on the other end. A magnet exerts a weak force of ∼1 pN to lift the paramagnetic bead off the surface, and laminar flow of buffer through the flow cell exerts a constant force of ∼3 pN on the bead and by extension, uniformly throughout the DNA tether. At this low force, ssDNA is entropically coiled, whereas dsDNA is stretched to nearly its crystallographic length (Fig. S1*C*). Conversion of ssDNA to dsDNA during primer extension can, therefore, be observed and tracked by extension of the DNA tether and movement of the coupled bead.

Glass coverslips were functionalized with a ratio of biotinylated PEG succinimidyl valerate:methyl-PEG succinimidyl valerate (Laysan Bio) of 0.75%:15% (wt/vol) in 0.1 M $NaHCO_3$ (pH 8.2) (10). Dried coverslips, stored under vacuum, were stable for several months.

Before an experiment, the functionalized coverslip surface was incubated with 0.2 mg mL^{-1} streptavidin (Sigma) in PBS for 30 min and then washed and incubated with blocking buffer (20 mM Tris·HCl, pH 7.5, 50 mM NaCl, 2 mM EDTA, 0.2 mg mL^{-1} BSA, 0.005% Tween 20) for an additional 30 min; 2–4 μL M13 substrate stock (∼5 nM; see above) was diluted with 500 μL blocking buffer and drawn into the flow cell at 0.025 mL min^{-1} with a syringe pump (Harvard Apparatus 11 Plus), allowing binding of DNA by the 5′-biotinylated ends to immobilized streptavidin sites. A stock of α-digoxigenin–functionalized polystyrene beads (tosyl-activated, 2.8-μm diameter; Dynal) was prepared as previously described (10); 2 μL bead stock was diluted with 500 μL blocking buffer and drawn into the flow cell at 0.025 mL min^{-1} to specifically bind the 3′-digoxigenin–labeled DNA substrates. Excess beads and DNA were removed from the flow cell by washing with 1 mL blocking buffer (>100 volumes) at 0.035 mL min^{-1}.

Immediately before the synthesis reaction, ∼150 μL replication buffer was introduced to exchange buffer. A solution of 500 μL replication buffer with replication proteins and nucleotides was added at 0.015 mL min^{-1}. A magnet exerting a weak force of ∼1 pN was used to lift the tethered paramagnetic beads off the surface; laminar flow at this rate through the flow cell exerts a constant force of ∼3 pN on the tether. After 2 min to allow the flow to stabilize, several hundred beads were visualized using dark-field microscopy through a 10× objective (Olympus) and imaged with a QIClick CCD camera (Q-Imaging). Data were recorded for 2,750 frames at 2 Hz using the software package Micro-Manager (www.micro-manager.org).

Primer extension on each individual molecule was observed by the motion of its bead in the direction of flow as the entropically coiled ssDNA was converted to extended dsDNA as previously indicated. Synthesis was not observed when dNTPs were excluded.

Single-Molecule Data Analysis. Individual beads were fit to 2D Gaussians and tracked with high accuracy (σ ∼ 20 nm) using the software package DiaTrack (Semasopht); beads nonspecifically stuck to the surface were used to subtract drift uniformly from all trajectories. Raw data for bead displacement in nanometers were converted into the number of base pairs synthesized using a calibration factor of 3.9 bp nm^{-1} determined by dividing the substrate length (7,249 bp) by the differential extension of ssDNA and dsDNA at the flow rate used (1,848 nm) (Fig. S1*C*).

To confirm the calibration factor and show the ability to observe a site-specific block of replication in the single-molecule primer extension assay, the dideoxy chain-terminated oligonucleotide 5′-GCT AAC GAG CGT CTT TCC AGA GCC TAA TTT GCC AGT TA-ddC-3′ (Integrated DNA Technologies) was annealed onto the M13mp18 single-molecule substrate ∼3,000 bp from the primer terminus. Synthesis was performed with T7 DNA polymerase exo$^-$, a gift from Charles Richardson (Harvard Medical School, Boston); primer extension terminated at the expected location (Fig. S1*D*).

Single-molecule trajectories were selected where the tethered DNA length increased in the direction of flow (y) but not the transverse direction (x). Trajectories that had a rapid simultaneous jump in both x and y represented sticking or unsticking of the bead to the surface of the flow cell and were excluded from analysis.

Synthesis trajectories were fit to segmented lines, with each segment corresponding to a Pol III event, a Pol IV event, or a pause using custom MATLAB code (Mathworks). Initial estimates for boundaries between segments were selected manually. The middle 80% of each region was then fit to a line, and new segment boundaries were determined from the intersection between adjacent segments. The processivity and rate for a segment are defined as the rise and slope, respectively.

Statistically significant synthesis events were defined as having a processivity greater than 3σ of the trajectory's noise (determined for individual trajectories but generally ∼200 bp); events were otherwise defined as pauses. A cutoff of 45 bp s^{-1} was used to assign significant synthesis events to Pol III (faster) or Pol IV (slower). This cutoff captures 93% of Pol III events and 95% of Pol IV events in experiments with individual polymerases.

Single-molecule data were binned to generate distributions and normalized to integrated counts, generating probability densities to facilitate comparisons. Fits of normalized histograms to one-term exponentials of the form $A \times \exp(-x/\lambda)$ for processivities (Fig. 1 and Figs. S3 and S7*B*) and $A \times \exp(-t/\tau)$ for pauses (Fig. 4 and Figs. S2, S6, and S7*A*) were determined using the MATLAB command fit, which generated the exponential fit constant (τ or λ).

Statistical comparisons were made between full datasets with the two-tailed Wilcoxon rank sum test using the MATLAB function ranksum and a significance level of $P = 0.05$.

Comparisons of Pause and Exchange Data. The slow rate of Pol IV (10.8 bp s^{-1} on average) implies that it takes ∼3σ/(10 bp s^{-1}) or ∼20 s to distinguish a Pol IV event from a pause. This lower bound for detection leads to undersampling of pauses less than 20 s for experiments with Pol IV alone and introduces noise in the determination of Pol III and Pol IV exchange times; however, these times are not similarly undersampled, because exchange is observed as a change in polymerase rate. We, therefore, binned the times in Fig. 4*A* and Fig. S2 *D*–*G* by 20-s intervals and when fitting curves to these distributions, excluded the first bin.

For statistical comparisons between full datasets in Fig. 4 and Figs. S6 and S7*A*, the Bonferroni correction for multiple sample comparisons was used to determine significance.

To exclude the possibility that exchange from Pol III to Pol IV in Fig. 4 *C* and *E* is only observed as more rapid because of undersampling of Pol IV pauses in Fig. 4*A*, we simulated unbiased pause times expected from Fig. 4*A* using the fit constant of 16.8 s and the MATLAB exponential random number generator exprnd. One hundred independent datasets were generated, each with $n = 51$ to match the dataset in Fig. 4*A*; all produced pause time distributions that were slower than the exchange data from Pol III to Pol IV on undamaged DNA ($P < 10^{-5}$ for each vs. Fig. 4*C*) and at the N^2-furfuryl-dG lesion ($P < 0.01$ for each vs. Fig. 4*E*).

As expected, a similar analysis simulating unbiased data from pause times for Pol IV in experiments with the single-cleft clamp, β^+/β^C (Fig. S2*G*, $\tau = 17.9$ s, $n = 165$), produced pause distributions slower than exchange data from Pol III to Pol IV ($P < 10^{-8}$ for each vs. Fig. 4*C* and $P < 10^{-3}$ for each vs. Fig. 4*E*); therefore, the equally valid comparison of exchange data with Pol IV

pauses with β^{+}/β^{C} does not affect our conclusion that Pol III and Pol IV simultaneously bind β and rapidly exchange.

Because pauses between rapid Pol III events are not similarly undersampled, this analysis was not required for Fig. 4 *B*, *D*, and *F*, and the statistical comparisons reported were from the data displayed in Fig. 4.

Bulk Primer Extension Reactions. Running start bulk primer extension reactions (Fig. S5*A*) were performed using the template 5′-CTA CCT **X**TG GAC GGC TGC GA-3′ (**X** = N^2-furfuryl-dG or the dG control) annealed with the 5′-^{32}P-phosphorylated primer 5′-TCG CAG CCG T-3′ in replication buffer with either 50 nM Pol III or Pol IV; 30-μL reactions containing the primer template (20 nM final) were initiated by adding dNTPs (250 μM) and incubating at 37 °C. At the indicated times, 3 μL each reaction was added to 10 μL stop buffer (50 mM Tris·HCl, pH 7.5, 25 mM EDTA, 0.5% SDS). The control reaction lacking dNTPs was stopped after 15 min. Samples were separated on a 12% (wt/vol) urea-PAGE gel, and the dried gel was exposed to a phosphor screen and imaged with a Personal Molecular Imager (BioRad).

Modeling of the Structure of a Pol III–Pol IV-β Complex. Fig. S9, prepared in PyMOL (Schrödinger), was based on a previously published model of the closed Pol III αεθ complex bound to DNA and β derived from structures of individual subunits and constraints from NMR, small-angle X-ray scattering, and cross-linking (11). The structure of Pol IV (Protein Data Bank ID code 4IR9) (12) was docked onto the rim site of β using the cocrystal structure of the Pol IV little finger domain bound to β (Protein Data Bank ID code 1UNN) (13). Docking resulted in a minor clash with the fingers domain of the Pol III α-subunit at residue 95 of Pol IV but no other clashes. The clamp-binding motif of Pol IV is disordered in the Pol IV structure (12) but would be positioned to replace the α–clamp-binding motif on a transient release from the cleft.

1. Beuning PJ, Simon SM, Godoy VG, Jarosz DF, Walker GC (2006) Characterization of *Escherichia coli* translesion synthesis polymerases and their accessory factors. *Methods Enzymol* 408:318–340.
2. Maul RW, Ponticelli SK, Duzen JM, Sutton MD (2007) Differential binding of *Escherichia coli* DNA polymerases to the β-sliding clamp. *Mol Microbiol* 65(3):811–827.
3. Wijffels G, et al. (2004) Inhibition of protein interactions with the β_2 sliding clamp of *Escherichia coli* DNA polymerase III by peptides from β_2-binding proteins. *Biochemistry* 43(19):5661–5671.
4. Hamdan S, et al. (2002) Hydrolysis of the 5′-p-nitrophenyl ester of TMP by the proofreading exonuclease (ε) subunit of *Escherichia coli* DNA polymerase III. *Biochemistry* 41(16):5266–5275.
5. Oakley AJ, et al. (2003) Flexibility revealed by the 1.85 Å crystal structure of the β sliding-clamp subunit of *Escherichia coli* DNA polymerase III. *Acta Crystallogr D* 59(Pt 7):1192–1199.
6. Scouten Ponticelli SK, Duzen JM, Sutton MD (2009) Contributions of the individual hydrophobic clefts of the *Escherichia coli* β sliding clamp to clamp loading, DNA replication and clamp recycling. *Nucleic Acids Res* 37(9):2796–2809.
7. Tanner NA, et al. (2008) Single-molecule studies of fork dynamics in *Escherichia coli* DNA replication. *Nat Struct Mol Biol* 15(2):170–176.
8. Jarosz DF, Godoy VG, Delaney JC, Essigmann JM, Walker GC (2006) A single amino acid governs enhanced activity of DinB DNA polymerases on damaged templates. *Nature* 439(7073):225–228.
9. Delaney JC, Essigmann JM (2006) Assays for determining lesion bypass efficiency and mutagenicity of site-specific DNA lesions *in vivo*. *Methods Enzymol* 408:1–15.
10. Tanner NA, van Oijen AM (2010) Visualizing DNA replication at the single-molecule level. *Methods Enzymol* 475:259–278.
11. Ozawa K, et al. (2013) Proofreading exonuclease on a tether: The complex between the E. coli DNA polymerase III subunits α, epsilon, θ and β reveals a highly flexible arrangement of the proofreading domain. *Nucleic Acids Res* 41(10):5354–5367.
12. Sharma A, Kottur J, Narayanan N, Nair DT (2013) A strategically located serine residue is critical for the mutator activity of DNA polymerase IV from *Escherichia coli*. *Nucleic Acids Res* 41(9):5104–5114.
13. Bunting KA, Roe SM, Pearl LH (2003) Structural basis for recruitment of translesion DNA polymerase Pol IV/DinB to the β-clamp. *EMBO J* 22(21):5883–5892.

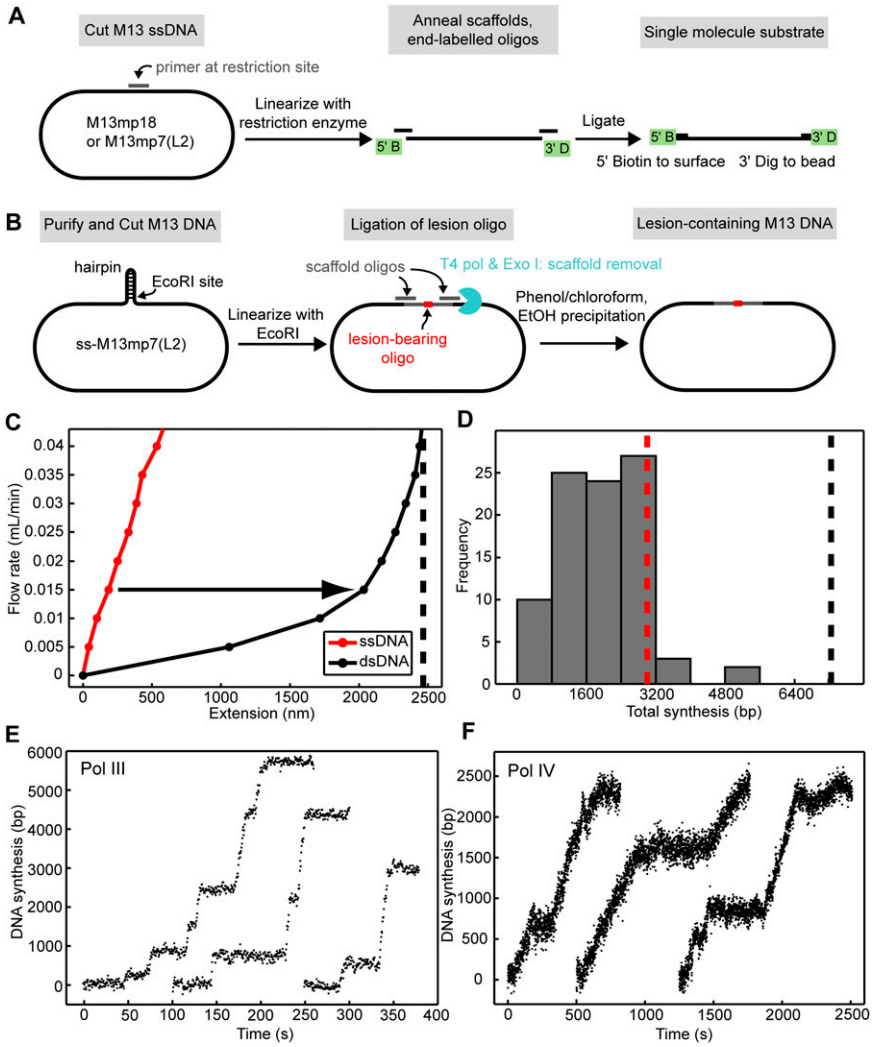

Fig. S1. A single-molecule primer extension assay. (*A*) A schematic of the construction of single-molecule substrates from M13 phage genomes: the circular ssDNA is linearized with a restriction enzyme and end-labeled using scaffold-mediated ligation. (*B*) A schematic of the generation of ssDNA containing a site-specific lesion: an internal hairpin is cleaved with EcoRI, and a chemically synthesized, lesion-containing oligonucleotide is ligated with scaffolds to recircularize the molecule. Excess primers and scaffolds are removed using T4 DNA polymerase and exonuclease I. (*C*) The differential extensions of ssDNA and dsDNA at increasing flow rates. dsDNA was generated from the single-molecule substrate stock using ϕ29 DNA polymerase (New England Biolabs). The conversion factor (3.9 bp nm^{-1}) used to calculate DNA synthesis from bead displacement was determined by dividing the total substrate length, 7,249 bp, by the difference in the extension of dsDNA and ssDNA at 0.015 mL min^{-1} (1,848 nm). (*D*) Annealing a 3′-dideoxy–terminated oligonucleotide onto the ssDNA substrate at the +3,000-bp position blocks synthesis by T7 DNA polymerase exo^{-} in 95% of trajectories (n = 91), confirming the conversion factor. The predicted location of the oligonucleotide block is marked with a dotted red line, and the full length of the substrate is marked with a dotted black line. Example trajectories for (*E*) Pol III (5 nM) and (*F*) Pol IV (30 nM). Initial time points are shifted for clarity; note different scales of axes.

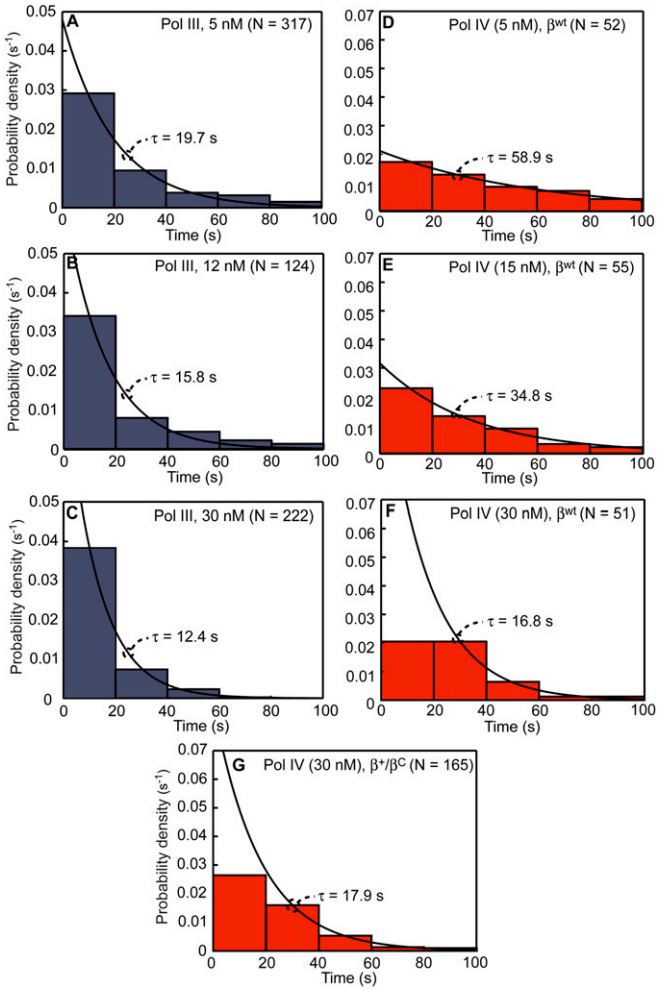

Fig. S2. Effects of polymerase concentration and the number of clefts on pausing. Pauses between polymerase synthesis events in single-molecule trajectories are exponentially distributed, suggesting a single rate-limiting step, and inversely related with concentration; increasing Pol III from (*A*) 5 to (*B*) 12 and (*C*) 30 nM or Pol IV from (*D*) 5 to (*E*) 15 and (*F*) 30 nM reduces these pause times. These data demonstrate that pauses observed during synthesis by Pol III or Pol IV alone represent dissociation of a polymerase followed by the diffusion-limited recruitment of another from solution. Association times (pauses) of Pol III are shorter because of a greater K_a for clamp binding measured in surface plasmon resonance experiments (1). Pauses observed in 30 nM Pol IV experiments with (*G*) the single-cleft clamp, β^{+}/β^{C}, are not significantly different from pauses observed in experiments with the WT clamp, β^{WT}. Observed pauses are, therefore, not caused by switching between two Pol IV molecules potentially bound to the same β dimer; τ represents the exponential constant for fits to pause distributions. The first bins of *D*–*G* are undersampled because of limits on the experimental resolution and therefore, were not used for fits.

1. Heltzel JM, Maul RW, Scouten Ponticelli SK, Sutton MD (2009) A model for DNA polymerase switching involving a single cleft and the rim of the sliding clamp. *Proc Natl Acad Sci USA* 106(31):12664–12669.

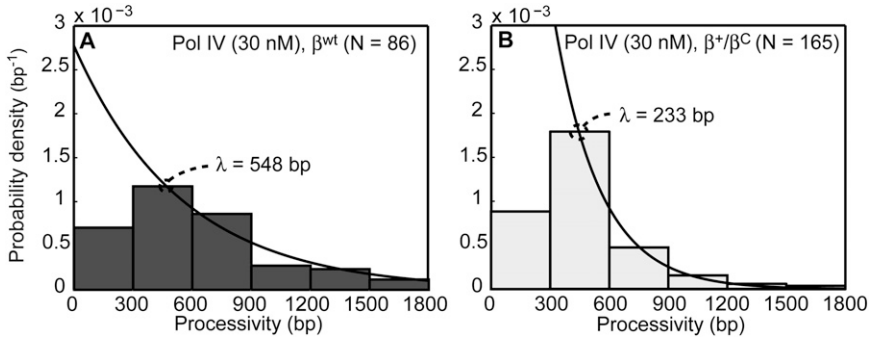

Fig. S3. Effect of the number of clefts available on Pol IV processivity. The observed processivity of Pol IV is greater in experiments with (*A*) β^{WT} than with (*B*) β^{+}/β^{C} ($P < 10^{-3}$), supporting structural data that two Pol IV molecules can bind a single β (1)—the apparent processivity is artificially increased by rapid, unresolvable switches between two polymerases bound to the clamp; λ represents the exponential constant for fits to processivity distributions. The first bins are undersampled because of limits on the experimental resolution and therefore, were not used for fits.

1. Bunting KA, Roe SM, Pearl LH (2003) Structural basis for recruitment of translesion DNA polymerase Pol IV/DinB to the β-clamp. *EMBO J* 22(21):5883–5892.

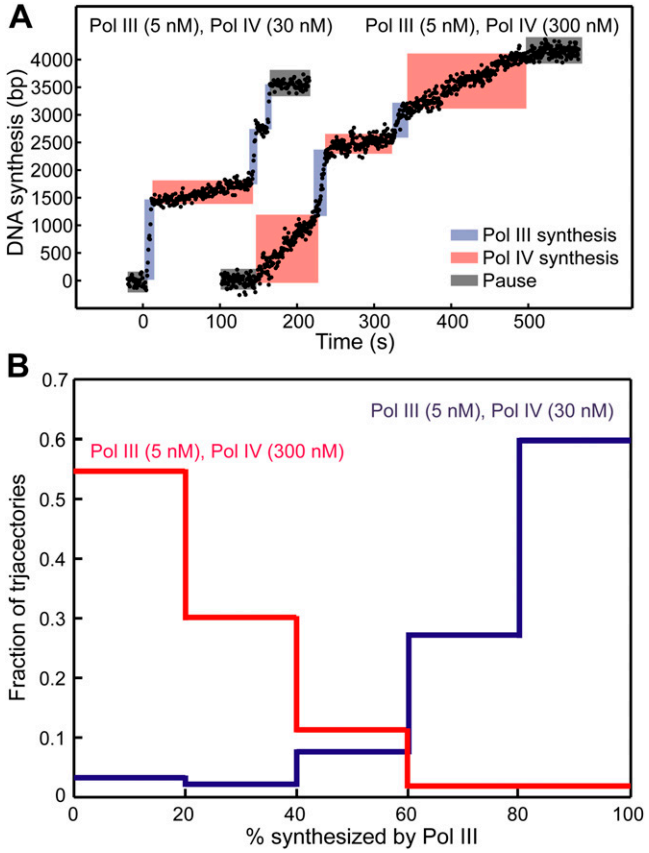

Fig. S4. Effects of increasing concentrations of Pol IV on competition with Pol III. (*A*) Example trajectories at a low and high ratio of Pol IV to Pol III with assignments. At high concentrations of Pol IV, individual pauses are no longer observable. (*B*) Distributions for the percent of synthesis completed by Pol III in individual trajectories in the presence of low (30 nM Pol IV, average of 78% Pol III synthesis; $n = 92$ trajectories) and high (300 nM Pol IV, 22% Pol III synthesis; $n = 53$) levels of Pol IV.

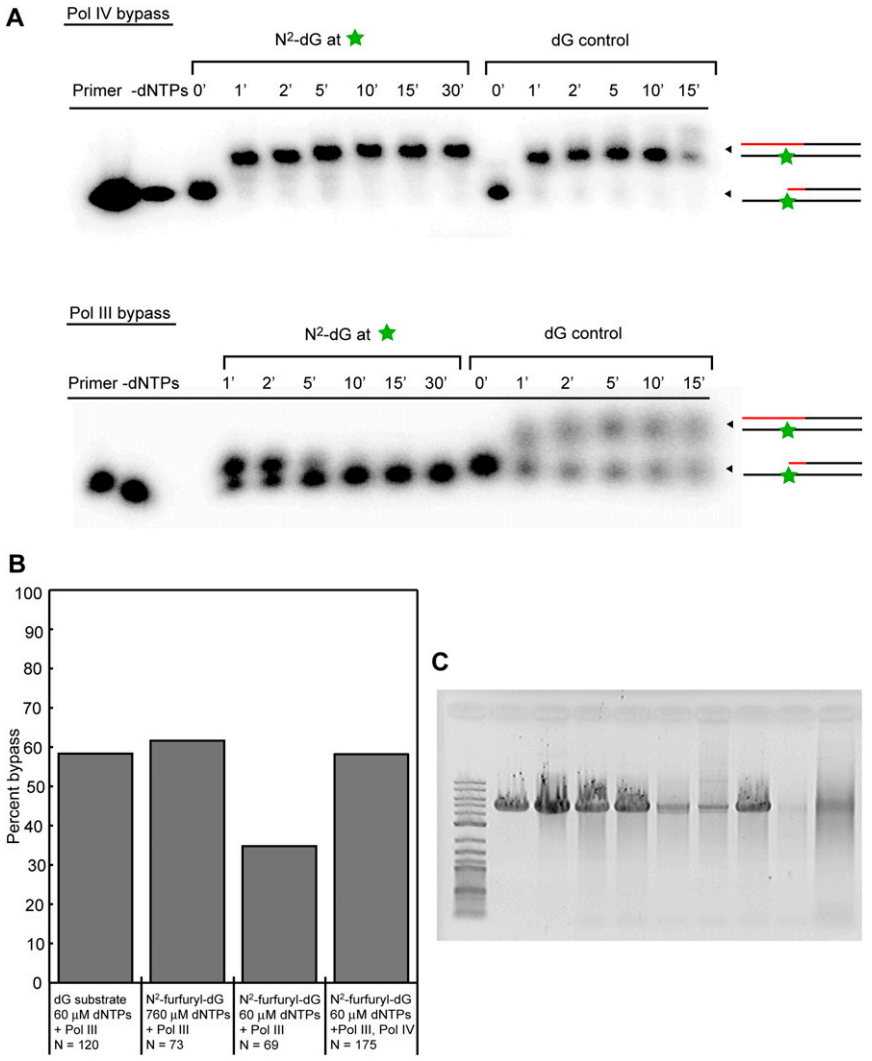

Fig. S5. Distributive and processive synthesis on templates containing a site-specific N^2-furfuryl-dG lesion. (*A*) A time course for distributive synthesis (in the absence of β) by Pol III or Pol IV on an oligonucleotide template with an N^2-furfuryl-dG (left side) or control dG (right side) base at the +3 position from the primer terminus. The lesion is a strong block for Pol III but rapidly bypassed by Pol IV. Arrows denote the location of the labeled 10-mer primer and the fully extended 20-mer product. Degradation of the primer by Pol III for the −dNTP control and on the lesion template is incomplete because of the short primer and the large footprint of the Pol III core. (*B*) The percentage of trajectories that bypasses the lesion site in single-molecule experiments. Bypass is defined as synthesis past the site plus 3σ of the noise (3,350 bp). Different conditions include lesion and control substrates, low and high dNTP concentrations, and with or without Pol IV. (*C*) Successive steps of preparation of lesion-containing M13 ssDNA; each lane of the agarose gel contains 700 ng DNA or the equivalent amount of the reaction unless otherwise specified. Lanes are numbered 1–10 from the left side: lane 1, 2-log ladder (5 μL; New England Biolabs); lane 2, M13mp18 ssDNA (New England Biolabs); lane 3, purified M13mp7L2 ssDNA; lane 4, after EcoRI digestion and subsequent purification; lane 5, after scaffold-mediated ligation with lesion-containing insert; lane 6, after treatment with T4 DNA polymerase and exonuclease I; lane 7, purified N^2-furfuryl-dG M13mp7L2. Treatment of mock-ligated (using scaffolds but no insert) substrate shows that digestion of the hairpin is nearly complete: lane 8, M13mp7L2 after the mock ligation; lane 9, after treatment with T4 polymerase and exonuclease I; lane 10, the same but loading 10 times the amount as lane 9.

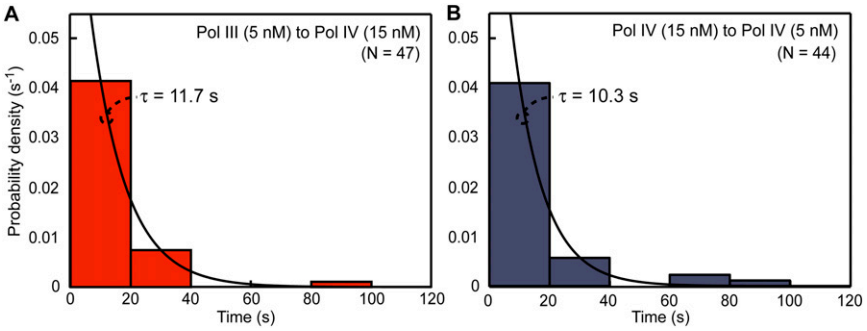

Fig. S6. Reducing the Pol IV concentration from 30 to 15 nM results in a timescale of exchange with Pol III statistically indistinguishable from Fig. 4*C*, despite the same dilution increasing the association time in experiments with Pol IV alone (Fig. S2 *E* and *F*). Exchange from (*A*) Pol III (5 nM) to Pol IV (15 nM) is more rapid than pauses in experiments with 15 nM Pol IV ($P < 10^{-5}$ vs. Fig. S2*E*); exchange from (*B*) Pol IV to Pol III remains rapid ($P < 10^{-7}$ vs. Fig. 4*A*).

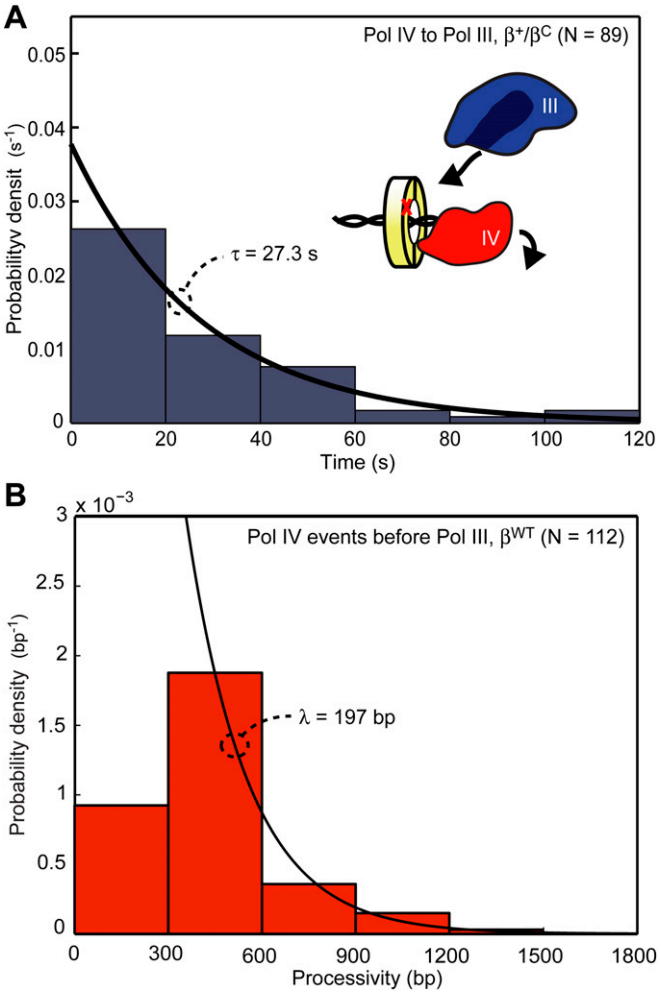

Fig. S7. Stoichiometry of Pol III and Pol IV on the clamp during rapid exchange. (*A*) Exchange from Pol IV (5 nM) to Pol III (30 nM) is diffusion-limited (*NS* vs. Fig. 4*B* and $P < 10^{-3}$ vs. Fig. 4*D*) in experiments with the single-cleft clamp, β^{+}/β^{C}, further showing that Pol III requires access to the free cleft to bind the clamp during Pol IV synthesis. (*B*) The processivity of Pol IV events preceding exchange to Pol III is less than the processivity of Pol IV alone (30 nM) with β ($P < 10^{-3}$ vs. Fig. S3*A*) and not significantly different from Pol IV with β^{+}/β^{C} (Fig. S3*B*), showing that a single Pol IV, at low concentrations, binds the clamp during exchange with Pol III.

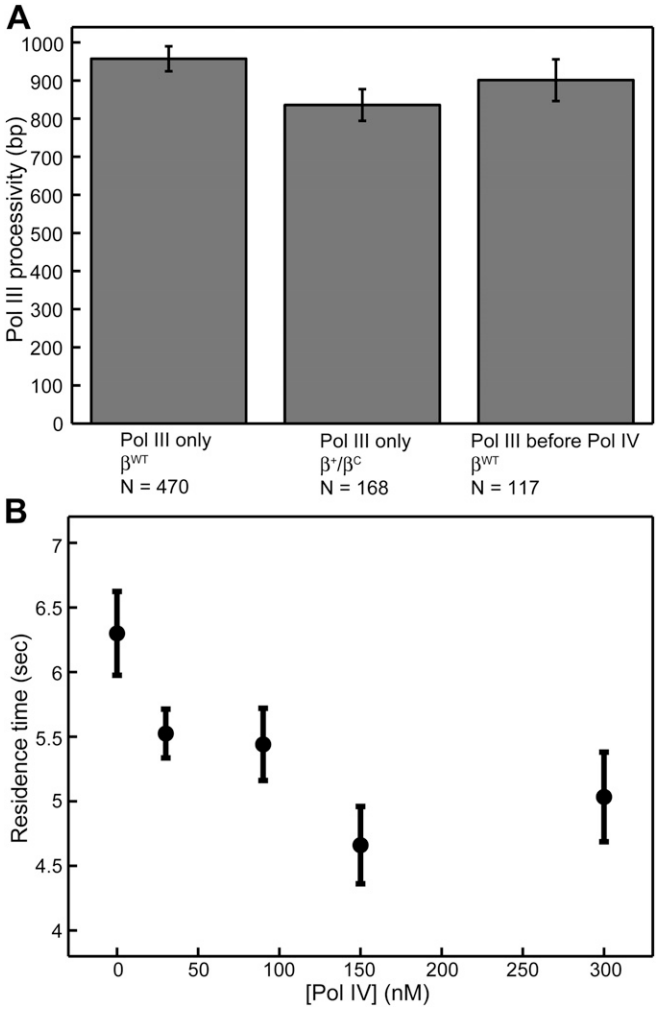

Fig. S8. Effects of Pol IV at low and high concentrations on Pol III stability. (*A*) Pol III processivity is modestly reduced by the absence of the ε–β contact and similarly reduced by the presence of Pol IV on the clamp, suggesting that Pol IV can compete with ε for a cleft. The average Pol III processivity in the following experiments (left to right): Pol III only (5 nM) in experiments with the WT clamp, β^{WT}; Pol III only (5 nM) with the single-cleft clamp, β^{+}/β^{C}, which eliminates binding by the weaker ε exonuclease subunit clamp-binding motif; and Pol III (5 nM) events that precede Pol IV (30 nM) events with the WT cleft. A similar reduction in Pol III processivity was previously observed in single-molecule leading strand experiments when the ε clamp-binding motif was weakened (1). (*B*) The average lifetime of Pol III on the clamp for individual synthesis events decreases with increasing concentrations of Pol IV. The lifetime for each event was determined by dividing the processivity by the rate.

1. Jergic S, et al. (2013) A direct proofreader-clamp interaction stabilizes the Pol III replicase in the polymerization mode. *EMBO J* 32(9):1322–1333.

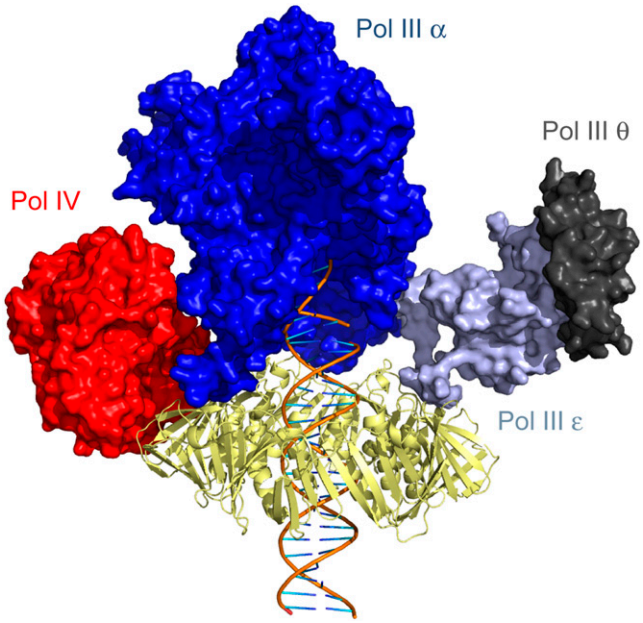

Fig. S9. Pol III and Pol IV bound to β (yellow), with Pol IV positioned at the rim site to capture the Pol III α clamp-binding motif during a transient release from its cleft. This model shows that concurrent binding of the two polymerases to the same protomer of β is consistent with structural data for Pol III and Pol IV and their clamp-binding modes. *SI Experimental Procedures* has details of model construction.

Table S1. Oligonucleotides (Integrated DNA Technologies) used to construct single-molecule substrates

Names	Sequences (5′ to 3′)
mp18-SalI	CTGCAGGTCGACTCTAGA
mp18-scaffold-1	GCGGGCAATATGTACCTCTAGAGGATCCCC
mp18-scaffold-2	ATGCCTGCAGGTCGAACTATGCGACTGGAC
mp7L2-AlwNI	AGCGCAGTCTCTGAATTTAC
mp7L2-scaffold-1	GCGGGCAATATGTACTCTCTGAATTTACCG
mp7L2-scaffold-2	GAATGGAAAGCGCAGACTATGCGACTGGAC
M13-3′-dig	GTACATATTGCCCGCAAAAAA-Dig
M13-5′-biotin	BioTEG-GTCCAGTCGCATAGT